A Family of Frontal Cyclones over the Western Atlantic Ocean. Part I: A 60-h Simulation

DA-LIN ZHANG

Department of Meteorology, University of Maryland, College Park, Maryland

EKATERINA RADEVA AND JOHN GYAKUM

Department of Atmospheric and Oceanic Sciences, McGill University, Montreal, Quebec, Canada

(Manuscript received 20 April 1998, in final form 14 August 1998)

ABSTRACT

Despite marked improvements in the predictability of rapidly deepening extratropical cyclones, many operational models still have great difficulties in predicting frontal cyclogenesis that often begins as a mesoscale vortex embedded in a large-scale (parent) cyclone system. In this paper, a 60-h simulation and analysis of a family of frontal cyclones that were generated over the western Atlantic Ocean during 13–15 March 1992 are performed using the Pennsylvania State University–National Center for Atmospheric Research mesoscale model with a fine-mesh grid size of 30 km. Although it is initialized with conventional observations, the model reproduces well the genesis, track and intensity of the frontal cyclones, their associated thermal structure and precipitation pattern, as well as their surface circulations, as verified against the Canadian Meteorological Centre analysis and other available observations.

It is shown that each frontal cyclone is initiated successively to the southwest of its predecessor in the cold sector, first appearing as a pressure trough superposed on a baroclinically unstable basic state in the lowest 150–300 hPa. Then, it derives kinetic energy from the low-level available potential energy as it moves over an underlying warm ocean surface (with weak static stability) toward a leading large-scale frontal zone and deepens rapidly by release of latent heat occurring in its own circulations. One of the frontal cyclones, originating in the cold air mass, deepens 44 hPa in 42 h and overwhelms the parent cyclone after passing over the warm Gulf Stream water into the leading frontal zone. These cyclones have diameters ranging from 500 to 1100 km (as denoted by the last closed isobar) and are spaced 1000–1400 km apart (between their circulation centers) during the mature stage. They begin to establish their own cold/warm frontal circulations once their first closed isobars appear, thus distorting the leading large-scale frontal structures and altering the distribution and type (convective versus stratiform) of precipitation.

It is found that the frontal cyclones accelerate and experience their central pressure drops as they move from high to low pressure regions toward the parent cyclone center, and then they decelerate and fill as they travel away from the parent cyclone. Their spatial and temporal scales, vertical structures, as well as deepening mechanisms, are shown to differ significantly from those typical extratropical cyclones as previously studied.

1. Introduction

The concept that extratropical cyclones tend to grow in frontal zones could be traced back to the polar front theory created by the famous Bergen School of cyclones in the 1920s. According to this theory, all extratropical cyclones originate in frontal zones, and so they can be thought of as frontal cyclones regardless of their characteristic spatial and temporal scales. Recent observational and theoretical studies (e.g., Reed 1979; Mullen 1979; Moore and Peltier 1987; Thorncroft and Hoskins 1990) revealed that the Norwegian conceptual cyclone model could be classified into two spatial regimes with quite different characters: one large-scale regime at a scale of greater than the Rossby radius of deformation or 3000 km and the other mesoscale regime (Orlanski 1975) in the range of 500–2000 km. The majority of the previous studies have been concerned with the growth of large-scale baroclinic waves at a timescale of a couple of days or more (see the recent reviews by Reed 1990; Hoskins 1990; Uccellini 1990). For the mesoscale regime, cyclones tend to develop along a cold front within a large-scale cyclone system or a ''parent'' cyclone. The cold front is then distorted by a single or multiple mesoscale depressions, forming a frontal wave that may grow with an *e*-folding time of one day or so (Moore and Peltier 1987; Joly and Thorpe 1990b). Even

Corresponding author address: Dr. Da-Lin Zhang, Department of Meteorology, University of Maryland, Room 2213, Space Science Building, College Park, MD 20742-2425.
E-mail: dalin@atmos.umd.edu

though they form in strong baroclinic zones, these secondary cyclones tend to be shallower than their large-scale counterparts. Therefore, the notion of *frontal or secondary cyclogenesis* is used here to imply *the cyclogenesis in the lowest 100–400 hPa with a diameter of 500–2000 km along a large-scale cold front with a parent cyclone in the polar region.*

Frontal cyclones have been found to occur in middle and higher latitudes over the globe. For instance, satellite photographs of North America and its coastal regions often reveal the existence of comma-shaped cloud patterns associated with subsynoptic-scale or secondary cyclones in polar airstreams (Mullen 1979, 1982; Bosart and Sanders 1991). Similar features have also been noted over the Pacific (Reed 1979) and the Atlantic (Rasmussen 1981), along Baiu fronts in East Asia (Matsumoto et al. 1970; Yoshizumi 1977), and in association with polar lows in Europe (Harrold and Browning 1969; Schär and Davies 1990). While frontal cyclogenesis is a widespread weather phenomenon, the understanding and prediction of this type of mesoscale vortex still remains among the most serious challenges to atmospheric scientists (Parker 1998). Unlike the cyclogenesis in the large-scale regime that can be well described by quasigeostrophic baroclinic theory (Charney 1947; Eady 1949), our understanding of frontal cyclogenesis is hampered mainly by (i) the lack of high-resolution data to resolve the processes leading to the secondary cyclogenesis, and (ii) the absence of theoretical models that could explain the initiation and growth of mesoscale disturbances in frontal zones. This has motivated the meteorological community to conduct the Fronts and Atlantic Storm Track Experiment (FASTEX) in January and February 1997 (Snyder 1996; Joly et al. 1997).

Observational studies of frontal cyclogenesis date back to Bjerknes and Solberg (1922), who noticed the tendency for secondary cyclones to develop in a family with each successive member occurring along the polar front to the southwest of its predecessor. Contemporary studies have focused on the formation of mesoscale vortices in relation to polar lows, coastal frontogenesis, and low- and upper-level jets using conventional observations that are generally too coarse to resolve the genesis and structures of frontal cyclones. Harrold and Browning (1969) studied the formation of mesoscale shallow depressions in the baroclinic zones as a result of upper-level traveling disturbances with positive vorticity advection. Reed (1979) and Mullen (1979) studied the structures and large-scale environments for a total of 24 wave cyclones that occurred behind cold fronts over ocean. They found that these mesoscale cyclones were initiated on the poleward side of upper-level jet streams as midlevel traveling disturbances moved close to the fronts. In a subsequent study, Mullen (1982) found numerous similarities of secondary cyclogenesis in the polar air mass between land and oceanic cases. In a case study of a small-scale polar-front cyclone, Ford and Moore (1990) noted that the storm tended to grow in response to favorable thermal advection along a low-level jet rather than to any significant upper-level forcing. Browning and Roberts (1994) and Browning and Golding (1995) examined the effect of upper-level high potential vorticity (PV) anomalies on the dry intrusions that appeared to determine the precipitation structure of frontal cyclones.

In contrast, frontal cyclogenesis has recently received a renewed interest in theoretical studies. These studies have shown the existence of unstable modes in the frontal zone that compare favorably with the spatial scale and growth rate of observed frontal cyclones, such as Moore and Peltier (1987,1990), Joly and Thorpe (1990a,b), and Schär and Davies (1990). These authors emphasized the growth of local baroclinic disturbances in the frontal zone, rather than from those originated in the cold or warm sector. Thorncroft and Hoskins (1990) showed that rapidly deepening frontal cyclones could result from the nonlinear interaction of an upper-level PV cutoff with an intense thermal gradient along a cold front during the final stages of a baroclinic wave life cycle. Other studies have been published to reconcile the observed mesoscale phenomena with conventional baroclinic instability (see the review by Parker 1998), which is often used to explain the growth of large-scale disturbances (Orlanski 1968, 1986; Kasahara and Rao 1972; Nakamura 1988), and with conditional instability of the second kind, which was originally developed to understand tropical cyclogenesis (Reed 1979; Mullen 1979).

Although frontal cyclogenesis has recently received considerable attention, few case studies have been performed, particularly using numerical simulations, to examine the detailed structures and evolution of these mesoscale phenomena and investigate the processes leading to secondary cyclogenesis. There are many questions that remain to be addressed. For example, is the frontal cyclogenesis different from typical extratropical cyclogenesis, apart from its spatial and temporal scales? Does its initial perturbation form in the frontal zone or in the cold (warm) sector? Of interest is that under certain circumstances, these baroclinically driven mesovortices can deepen rapidly and eventually dominate their parent cyclone. What then is the relationship(s) between frontal and parent cyclones? What are the basic ingredients contained in the large-scale circulations causing the frontal cyclogenesis? Therefore, detailed case studies on frontal cyclogenesis are necessary in order to provide a better understanding of the interaction of different processes leading to secondary cyclogenesis and improve our ability to predict the associated weather phenomena.

In this study, we investigate the formation of a family of six frontal cyclones that occurred over the western Atlantic Ocean on 13–15 March 1992 during the Canadian Atlantic Storms Program (Stewart 1991) primarily using a 60-h high-resolution ($\Delta x = 30$ km) simulation of the case with the Pennsylvania State Uni-

versity–National Center for Atmospheric Research (PSU–NCAR) Mesoscale Model version 4 (MM4; Anthes et al. 1987). This case is selected for this study because (i) there was a family of six secondary cyclones with diameters ranging from 500 to 1100 km along a large-scale front, and (ii) they were missed by the then operational models, such as the Nested Grid Model (NGM) in the National Centers for Environmental Prediction (NCEP) and the Regional Finite Element (RFE) model in the Canadian Meteorological Center (CMC). Moreover, one of the frontal cyclones, originating in the cold air mass, underwent explosive deepening (i.e., 44 hPa/42 h) and it eventually overpowered the parent cyclone. However, both the NGM and RFE models, initialized at 0000 and 1200 UTC 13 March, predicted a mesotrough at the end of the cyclone's life cycle and failed to reproduce other frontal cyclogenesis events. Thus, the present case provides a great opportunity to examine the mesoscale predictability of frontal cyclones and their initiating and deepening mechanisms. The objectives of the present paper are to (i) demonstrate the model predictability of the 13–15 March 1992 family of frontal cyclogenesis events out to 60 h using MM4 with an enhanced analysis as the model initial conditions, and (ii) document the three-dimensional structures and evolution of the frontal cyclones in relation to their parent cyclone as well as their interrelations. Model sensitivities to different physical processes will be presented in Part II of this series of papers (Zhang et al. 1999).

The next section provides a brief description of the main model features used for the present study. Section 3 shows the model initialization and initial conditions. The origin of the frontal cyclone that eventually overpowered the parent cyclone will be documented. Section 4 examines the structures and evolution of the frontal cyclone family from 0000 UTC 13 March to 1200 UTC 15 March 1992 and presents verification of the 60-h simulation against the CMC analysis and satellite observations. Section 5 describes the structures of upper-level flows in relation to the surface developments. A summary and concluding remarks are given in the final section.

2. Model description

An improved version of MM4, the PSU–NCAR three-dimensional, hydrostatic, nested-grid, mesoscale model (Anthes et al. 1987) is used for the present study. The fundamental features of this model include (i) a two-way interactive nested-grid procedure that allows incorporation of realistic topography (Zhang et al. 1986); (ii) use of the Kain–Fritsch (1990, 1993) cumulus parameterization scheme for the fine-mesh domain and the Anthes-type cumulus scheme for the coarse-mesh domain; (iii) an explicit moisture scheme containing prognostic equations of cloud water (ice) and rainwater (snow), as described in Hsie et al. (1984), Zhang (1989), and Dudhia (1989); (iv) the Blackadar high-resolution boundary layer parameterization (Zhang and Anthes 1982); and (v) specification of the coarse-mesh outermost lateral boundary conditions by linearly interpolating 12-h observations (Perkey and Kreitzberg 1976).

The nested-grid ratio is 1 to 3, with a fine-mesh length of 30 km and a coarse-mesh length of 90 km. The (x, y, σ) dimensions of the coarse and fine meshes are $89 \times 75 \times 19$ and $139 \times 109 \times 19$, respectively, and they are overlaid on a polar stereographic map projection true at 60°N. The vertical coordinate, σ, is defined as $\sigma = (p - p_t)/(p_s - p_t)$, where p is pressure, p_s is the surface pressure, and p_t is the pressure at the top of the model atmosphere (in the present case $p_t = 70$ hPa). The 20 σ levels are 0.0, 0.05, 0.1, 0.15, 0.206, 0.263, 0.321, 0.38, 0.44, 0.501, 0.562, 0.619, 0.676, 0.733, 0.789, 0.845, 0.901, 0.957, 0.99, 1.0, which give the 19 σ layers of unequal thickness. Figure 1 shows the nested-grid domains of the fine and coarse meshes. Both computational domains cover the area of genesis and subsequent development of the frontal cyclone family as well as the data-rich area to the west where upstream disturbances affecting the cyclones form. A large coarse-mesh domain is used here to minimize the influence of lateral boundaries on the model predictability of the present frontal cyclogenesis family occurring over the western Atlantic Ocean.

The only improvement to the standard version of MM4 for the present case study is related to the calculation of surface fluxes of heat, moisture, and momentum over ice surfaces, which are defined as ocean or lake surfaces with a temperature of less than −2°C. In this case, no upward surface heat and moisture fluxes are allowed. A surface roughness length of 1 cm is used in the calculation of surface momentum fluxes. This treatment is critical in reproducing the low-level temperature structures over Hudson Bay, the Labrador Sea, and along ice edges.

3. Model initialization and initial conditions

The model is initialized at 0000 UTC 13 March 1992 with data from conventional observations, following the method described in Zhang et al. (1986), and then integrated for 60 h. The NCEP 2° latitude–longitude global analysis was first interpolated to the model coarse mesh as a first guess and then enhanced with rawinsonde observations through a successive-correction method (Benjamin and Seaman 1985). Over the ocean, modifications of the NCEP analysis were limited to the use of ship and buoy observations; this procedure improves primarily the representation of the sea level pressure field. Sea surface temperature (SST) was obtained from NCAR's U.S. Navy tape. An inspection of Fig. 1 reveals that the frontal cyclones under study moved along the southern edge of the pronounced SST gradients and eventually into the colder water to the northeast. The fine-mesh data were obtained by interpolating the en-

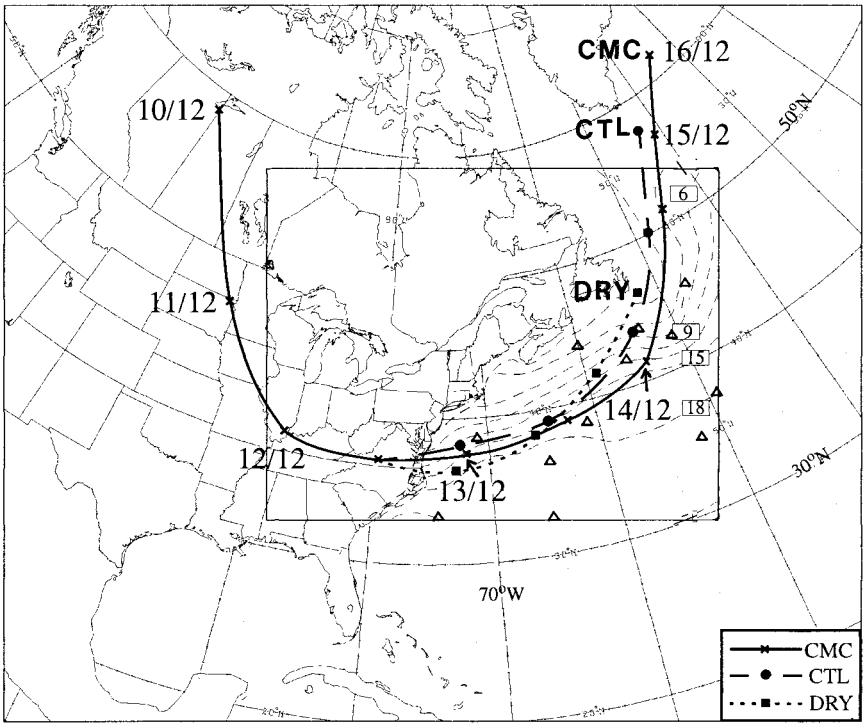

FIG. 1. Nested-grid domains with the fine mesh denoted by the internal frame. Sea surface temperature (dashed) is given at intervals of 3°C over the fine-mesh domain. Tracks of the major frontal cyclone (MFC) from the CMC analysis (solid) over a 6-day period with date/hour given, the 60-h simulation (CTL, thick dashed), and the 48-h dry simulation (DRY, dotted) are shown. Locations of available ship and buoy reports at 1200 UTC 14 Mar 1992 over the fine-mesh domain are given by open triangles. Latitudes and longitudes are given every 10°.

hanced coarse-mesh fields. No balancing between the mass and wind fields was done, but the vertically integrated divergence was set to zero initially in order to minimize gravity wave noise in the first few hours of integration.

Figure 2 shows surface maps at the model initial time, that is, the enhanced NCEP analysis[1] at 0000 UTC 13 March 1992 (henceforth 13/00), as well as the CMC analysis at 12 h earlier (i.e., 12/12). Because of its 6-hourly time resolution, the CMC analysis will be used in subsequent discussions. At 12/12, the large-scale circulation was seen to be dominated by a large-scale low pressure system, with a central pressure of 980 hPa, positioned over the south-central portion of Quebec. This low, hereafter referred to as the parent cyclone (P), had experienced 12-hPa deepening as it moved from central Ohio during the previous two days (not shown). It could be traced back farther to an intense cyclone in southwestern Kansas at 09/12 (see Fig. 4 in Wang et al. 1995) during the Storm Operational and Research Meteorology–Fronts Experiment Systems Test. There were at least three visible pressure perturbations under the influence of the cyclonic flow: one associated with a primary cold front extending southeastward along the east coast of Newfoundland into the ocean, followed by a surface (trough–ridge) short wave that was evident along the coast of the middle Atlantic states and a secondary mesolow centered near the common border of Illinois, Kentucky, and Missouri, as marked by (M). This mesolow could be traced back to a surface cyclone two days earlier in northern Saskatchewan (see Fig. 1); it is similar to a ''polar low'' as in Reed (1979) and Mullen (1982) and had not changed its intensity over the two-day period.

It is important to note (i) a cold polar air surge to the east of the Rocky Mountains that had seemed to force the *mesolow* (M) to move rapidly southeastward, and (ii) a slowly moving intense baroclinic zone offshore that was left behind the primary cold front within which the *short-wave system* (N) was located (Fig. 2a). As will be seen later, the secondary low pressure perturbations developed into two intense frontal cyclones within the parent cyclone system as they advanced into the leading cold frontal zone. So they will be hereafter referred to as the major (M) and the northern (N) frontal cyclones or MFC and NFC, respectively, since the former eventually overpowered the parent cyclone. A third frontal

[1] The NCEP analysis was used to generate the model initial conditions for the present study because the current PSU–NCAR modeling system could not process the CMC analysis.

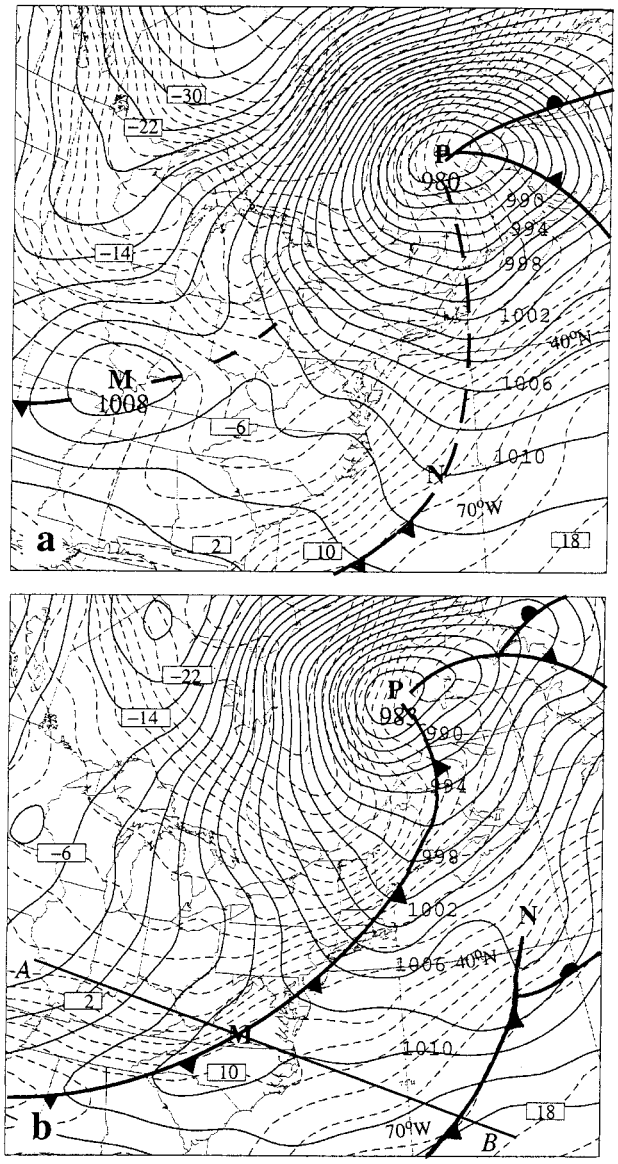

FIG. 2. Sea level pressure (solid, every 2 hPa) and surface temperature (dashed, every 2°C) (a) from the CMC analysis at 1200 UTC 12 Mar and (b) the enhanced NCEP analysis at 0000 UTC 13 Mar 1992 (i.e., the model initial conditions). P, M, N, and S, mark the centers of the parent, major, northern, and southern cyclones, respectively; similarly for the rest of figures. Line AB in (b) shows the location of vertical cross section used in Fig. 4.

cyclone emerged at 14/12 to the south of the MFC, so named the southern frontal cyclone (S) or SFC. Another three frontal cyclones developed prior to 15/12.

At the model initial time (i.e., 13/00), the mesolow (M) weakened into a mesotrough (with a weak vorticity center) after it passed over the Appalachians (see Figs. 2b and 4). This trend of weakening upon approaching the Appalachians has also been noted by O'Handley and Bosart (1996) in a climatological study of cyclones crossing the mountains. Meanwhile, the rapid movement of the cold polar air mass resulted in the formation of a new large-scale cold front extending along the East Coast through North Carolina into Texas, whereas the surface-based short-wave trough (N) began to amplify in the baroclinic zone as it moved rapidly northeastward. The MFC would grow out of the vorticity center in the frontal zone over North Carolina after it moved offshore. In contrast, the parent cyclone showed a sign of weakening and slower northeastward movement during the 12-h period.

Upper-level large-scale circulations were also dominated by the parent cyclone (see Fig. 3), which exhibits a vertically stacked structure up to 250 hPa. This again indicates the existence of little baroclinic support for the further deepening of the parent cyclone, and, indeed it began to fill. Note the presence of a ring of high PV exceeding 3.5 PVU (1 PVU = 10^{-6} m^2 K s^{-1} kg^{-1}) on the cyclonic side of the jet stream (Fig. 3b), with near-zero PV in the central weak-flow region. This PV ring is indicative of the tropopause depression and represents the interface between the tropical and polar air masses. Of particular interest is that the 6-day track of the MFC resembles closely the distribution of the PV ring (cf. Figs. 1 and 3b), suggesting the important role of its induced flow in steering the movement of the frontal cyclone (Hoskins et al 1985).

A southwest–northeast-oriented short-wave trough T_1, tilting rearward, was closely associated with a PV center that was supported by a direct secondary transverse circulation in the left entrance region of the jet streak (see Fig. 4). This trough, propagating together with the surface mesolow, had weakened significantly during the previous two days (not shown). Another trough, T_2, associated with the NFC, was also evident; but it was very weak and exhibited little vertical tilt. The 850-hPa map displays moderate cold advection occurring in the vicinity of trough T_1 over the southeastern states, with little thermal advection ahead in spite of the intense thermal gradients (Fig. 3d). However, the intense south–north thermal gradients accounted for the development of an especially strong westerly jet streak at 250 hPa (Fig. 3a); its peak intensity, located at the Carolinas' border, was greater than 80 m s^{-1}.

It is apparent that the MFC was now located over a region of positive vorticity advection (Fig. 3) and near the core of the jet streak on its cyclonic side (Fig. 3a), a scenario similar to that described by Reed (1979) and Mullen (1979, 1982). As Fig. 1 shows, the simulated MFC moves at about 15 m s^{-1} along the westerly jet streak after it moved offshore and then accelerates rapidly to 25 m s^{-1} northeastward away from the exit region of the jet streak. Thus, the jet streak–induced indirect transverse ageostrophic circulation in its exit region, as described by Uccellini and Johnson (1979), did not seem to have an important impact on the genesis of the MFC, but it might assist the development of the NFC.

A vertical cross section of deviation height and potential temperature through the MFC is given in Fig. 4,

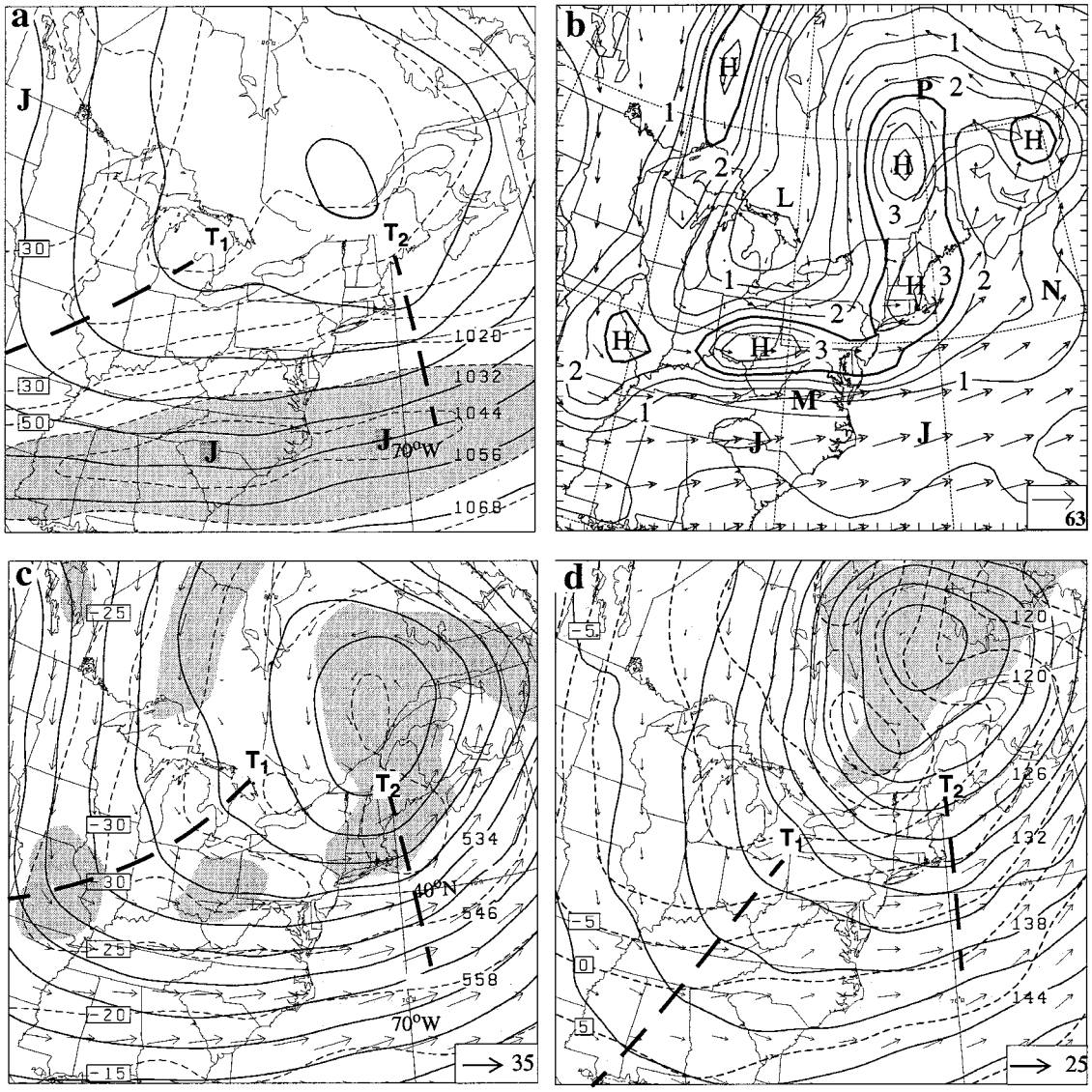

FIG. 3. The enhanced NCEP upper-level analysis at the model initial time (i.e., 0000 UTC 13 Mar 1992): (a) 250-hPa height (solid, every 12 dam) and isotachs (dashed, every 10 m s^{-1}) with the speeds >60 m s^{-1} shaded; (b) 400-hPa PV at intervals of 0.5 PVU superposed with wind vectors; (c) 500-hPa height (solid, every 6 dam) and isotherms (dashed, every 5°C), superposed with flow vectors with absolute vorticity $>15 \times 10^{-5}$ s^{-1} shaded; (d) 850-hPa height (solid, every 3 dam) and isotherms (dashed, every 5°C), superposed with flow vectors with absolute vorticity $>15 \times 10^{-5}$ s^{-1} shaded. Inset indicates the scale of horizontal wind speed (m s^{-1}). J marks the center of the jet streak, and T1 and T2 indicate the troughs associated with the MFC and NFC, respectively.

which shows a deep layer of strong vertical wind shear (above 800 hPa) associated with the upper-level jet streak. (The deviation height is obtained by subtracting the pressure-level average within the cross section.) The cold frontal zone near (M) was seen to be quite shallow, only up to 750 hPa, with relatively weak (moderate) static stability ahead (behind). The prefrontal weak static stability was closely related to the presence of the underlying warm Gulf Stream water, and thus tended to render it more susceptible to upright convection in the presence of a favorable forcing. Again, the MFC was located downstream of the upper-level trough that tilted westward with height, and it was about to move over the Appalachians into the region with decreasing static stability. Apparently, both the upper-level trough and the low-level weak static stability are favorable for the genesis of the MFC and other frontal cyclones.

4. Case description and simulation

In this section, we describe the sequence of a family of secondary cyclogenesis in relation to their parent cyclone during a 60-h integration period (from 13/00–00 to 15/12–60 March 1992), using the CMC analysis,

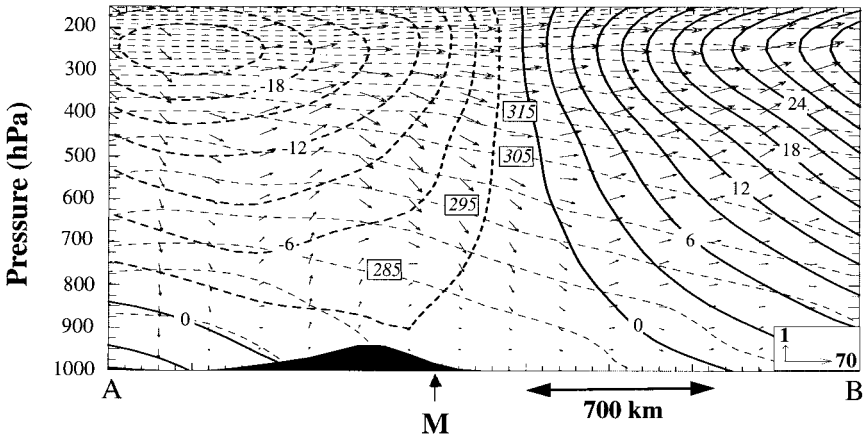

FIG. 4. Vertical cross section of deviation height (heavy solid and dashed, every 3 dam) and potential temperature (light dashed, every 5 K), superposed with alongplane wind vectors, which is taken along line AB given in Fig. 2b at the model initial time (i.e., 0000 UTC 13 Mar 1992). Inset indicates the scale of vertical (Pa s^{-1}) and horizontal (m s^{-1}) motions.

the model simulation, and satellite observations. In view of the limited data over ocean, only simulated surface maps will be verified against the CMC analysis and other available data. Then, we can use the simulation results to study nonobservable features and gain insight into how large-scale disturbances interact with the surface circulations in influencing the multiple secondary cyclogenesis events.

For economy of space, we will focus below on the MFC genesis scenarios, with less attention given to the other secondary genesis events. Figures 1 and 5 compare, respectively, the tracks and central pressure traces of the MFC between the MM4 simulation and the CMC analysis. An inspection of the model simulation reveals that the first closed isobar of the MFC begins to emerge at 18 h into the integration, that is, 1800 UTC 13 March (henceforth 13/18–18), after it moved offshore. It is apparent from Fig. 1 that the predicted track follows closely the analyzed one, only with some systematic deviation to the west. The maximum departure between the two tracks is less than 120 km at the end of the 60-h integration period, during which the MFC has traveled more than 4000 km from North Carolina to the south of Greenland.

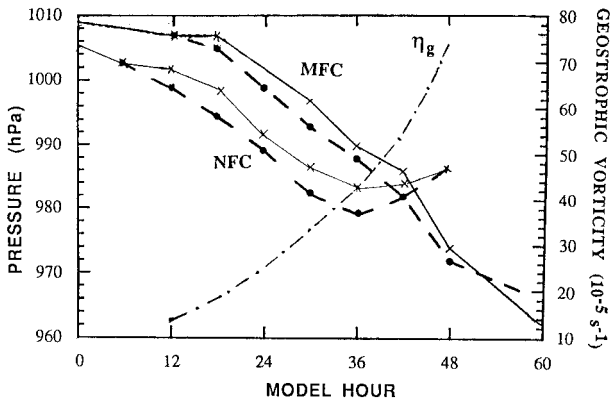

FIG. 5. Time series of the central sea level pressure of the MFC and the NFC from the CMC analysis (solid, CMC) and the simulation (dashed, CTL). Time series of the simulated absolute geostrophic vorticity (η_g, 10^{-5} s^{-1}) averaged between 900 and 1000 hPa for the MFC is also shown (dot–dash).

Similarly, the model simulates well the slow growth of the MFC during the first 18-h integration and its subsequent rapid deepening; so its life cycle can be divided into the genesis and rapid deepening stages accordingly. In particular, the model replicates the observed deepening rate of 44 hPa in 42 h between 13/18–18 and 15/12–60, which qualifies it as an ''oceanic bomb'' in accordance with Sanders and Gyakum (1980). The nine-point averaged 6-hourly *e-folding time*, computed from the simulated quasigeostrophic absolute vorticity (η_g, see Fig. 5) at the cyclone center in the lowest 100 hPa [$t_e = -(\nabla \cdot \mathbf{V})^{-1} = \Delta t\{\ln[\eta_g(t_1)/\eta_g(t_0)]\}^{-1}$, where $\Delta t = t_1 - t_0 = 6$ h], *varies from 18.4 h* (during the 12–18-h integration) *to 24.0 h* (during the 36–42-h integration) *with an average value of 21.8 h.* Note that this timescale is close to the theoretical evaluation of frontal cyclogenesis, for example, by Moore and Peltier (1987) and Joly and Thorpe (1990b), but using dry dynamic models in which both latent heat release and surface processes were ignored. This similar *e*-folding time between our moist run and those dry models is attributable to the fact that the amplifying impact of latent heating tends to be offset by the dissipating effect of surface friction. Obviously, to obtain a more realistic estimate of the growth rate, theoretical studies of frontal cyclogenesis have to include the effects of both the diabatic heating and the surface friction. This point will be further addressed in Part II of this series of papers.

As for the NFC, the model appears to overpredict its central pressure drop between the 24- and 36-h integrations (see Fig. 5). This overprediction could be at-

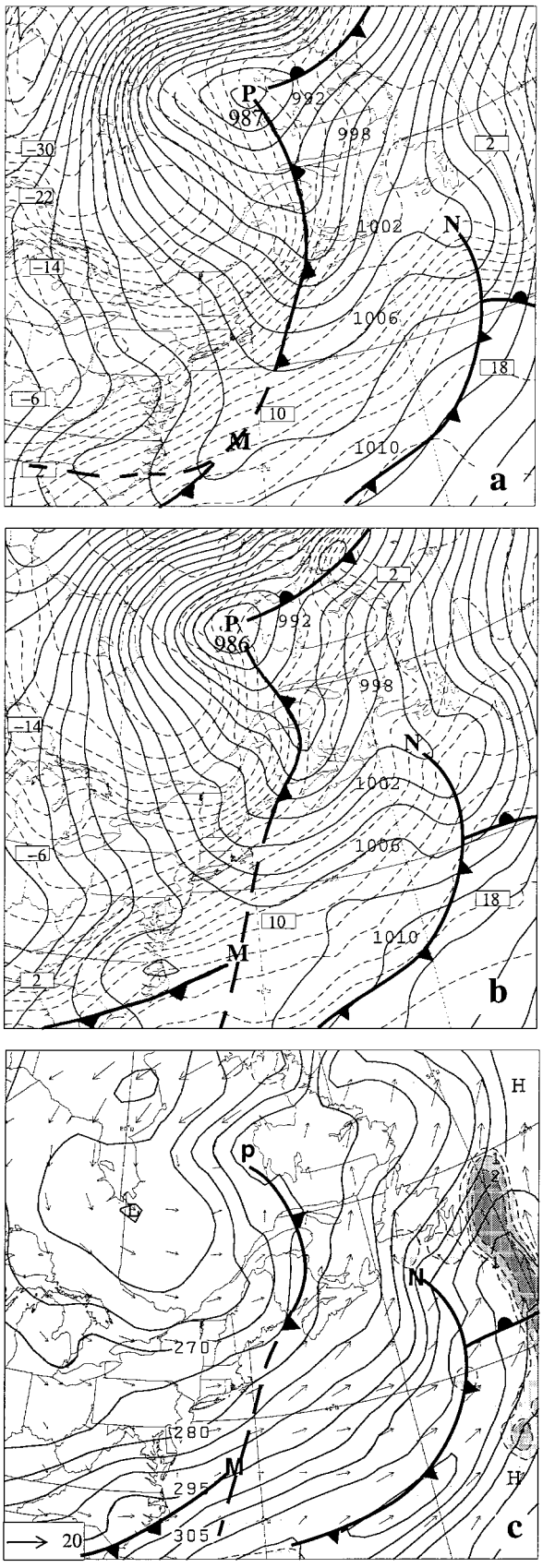

tributed partly to the observations over ocean that are too coarse to resolve such a mesoscale feature (see Fig. 1), and partly to the position with respect to the parent cyclone center, as will be seen later. Nevertheless, the model captures fairly well the life cycle of the NFC, which underwent 16-hPa deepening in 36 h; its circulation was eventually absorbed by the MFC.

The following analyses focus on the multiple frontal cyclogenesis events and their associated circulation characteristics in relation to the parent cyclone. Figures 6 and 8–11 compare the 12-hourly simulated surface maps to the CMC analysis over subdomains moving with the MFC system. We have shown in Fig. 2b that the rapid southeastward movement of an intense baroclinic zone assisted the organization of a large-scale cold front along the East Coast at 13/00–00. However, this cold front changed its thermal structure [i.e., in the dashed trough region around (M) in Fig. 6a] 12 h later after it merged with the slow-moving cold air mass offshore. The sign of the dissipated mesolow or MFC was still visible after the merging, as evidenced by a local Laplacian pressure maximum. Of importance is that *the merging allowed stronger warm advection to occur ahead of the trough axis by cross-isobaric flows*, more intense in the vicinity of the MFC. With the intense cold advection already present behind, this baroclinic setup is clearly favorable for the growth of the MFC; this thermal advective effect will be quantified in Part II. In contrast, the parent cyclone (P) continued to decay as it traveled slowly northward.

The model reproduces reasonably well the intensity and movement of the parent cyclone, the orientation of the large-scale frontal trough, the intense thermal gradients across it, as well as the MFC to the south (cf. Figs. 6a,b). A model-derived sounding at the MFC center (see Fig. 7a) shows that the cyclogenesis is about to take place in a deep baroclinically unstable state, as indicated by the intense westerly shear in the vertical. The atmospheric stratification is characterized by *a well-mixed boundary layer up to 850 hPa* as a result of the colder air overrunning the warm Gulf Stream water, and a deep layer of warming and drying associated with the tropopause depression above 400 hPa (Fig. 3b). Obviously, the low-level near-neutral stability assists the subsequent development of mesoscale storms and convective precipitation. During this 12-h period, however, the model produces little precipitation associated with the intensifying frontal trough, suggesting that *dry dynamics dictates the genesis stage of the MFC*; this will be

←

FIG. 6. Sea level pressure (solid, every 2 hPa) and surface temperature (dashed, every 2°C) at 1200 UTC 13 Mar 1992 (13/12–12) from (a) the CMC analysis and (b) 12-h simulation. (c) The 900-hPa equivalent potential temperature θ_e (solid, every 5 K) superposed with wind vectors and hourly precipitation rates (shading–dashed lines are contoured at 0.5, 1, 2, and 5 mm h^{-1}) from the 12-h simulation. Inset indicates the scale of horizontal winds (m s^{-1}).

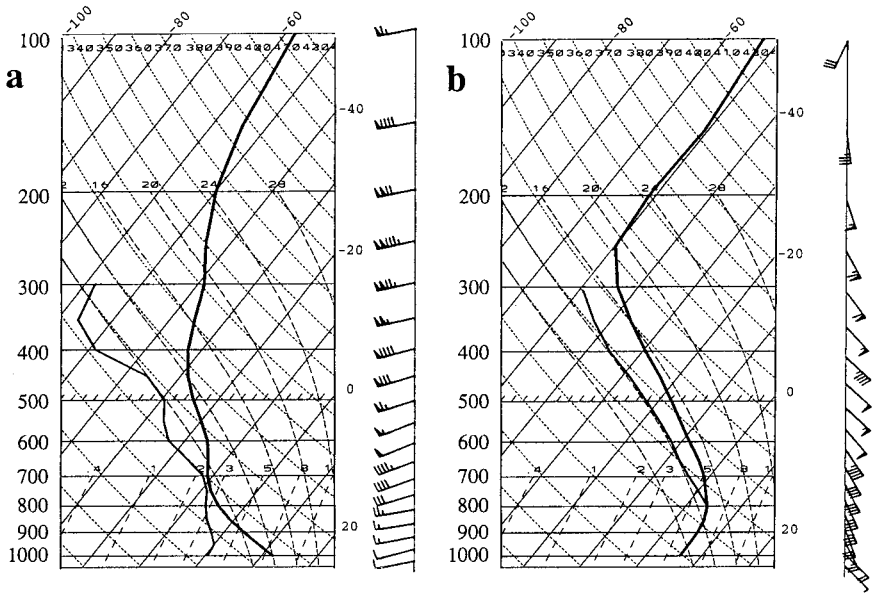

FIG. 7. Skew *T*–log*p* diagrams taken at the center of the MFC (i.e., at point M) from (a) 12-h and (b) 48-h simulations. A full (half) barb is 5 (2.5) m s^{-1} and a pennant is 25 m s^{-1}.

further shown through sensitivity simulations in Part II. The model-produced precipitation occurs mainly ahead of the leading primary cold front to the east (Fig. 6c), which is in agreement with the satellite observations (not shown).

Likewise, the model reproduces well the movement of the NFC, and its associated warm and cold frontal structures ahead of the large-scale frontal trough. This successful predictability of the NFC at nearly the right location and the right time results primarily from the initial superposition of the surface trough in a baroclinic unstable state plus the upper-level support associated with the ring of high PV, since few upper-air observations were available to resolve the NFC in the model initial conditions.

At 14/00–24, both the CMC analysis and the simulation show the growth of a closed mesolow (i.e., the MFC) out of the mesotrough in the frontal zone (cf. Figs. 6 and 8). It is important to note that *both the MFC and the NFC form in the cold air mass and then deepen in the leading frontal zone.* To our knowledge, these kinematic processes of frontal cyclones have never been documented by any of the previous observational studies. It is found from the simulation that once a frontal cyclone develops its first closed isobar, it begins to establish its own warm–cold frontal circulations. It distorts substantially the leading frontal structures as it moves close to the frontal zone (cf. Figs. 8–10). In the case of the MFC, the leading large-scale frontal identity has been replaced by the MFC-induced circulations, at least in the lower troposphere. Of interest is that this distortion alters gradually the distribution and type (convective versus stratiform) of precipitation along the leading baroclinic zone. Specifically, a high-θ_e tongue coupled with alongfront flows is located ahead of the primary cold front (Fig. 8c), which clearly feeds energy into the cyclone systems in the form of latent and sensible heat along the fronts. Because of the frontal distortion, one stratiform region with moderate precipitation develops near the cyclone center along the newly formed warm fronts (cf. Figs. 6c and 8c), instead of just a single elongated convective rainband ahead of the leading frontal zone as seen at 13/12–12 (Fig. 6c). In the present case, the more rapid deepening of all the frontal cyclones (i.e., MFC, NFC, and SFC) always coincides with intense stratiform precipitation to the north (see Fig. 12a) where statically stable stratification prevails (Fig. 7b).

Meanwhile, the NFC continues to deepen as it moved into the southern Labrador Sea under the influence of the general cyclonic flow. Its central pressure even becomes deeper than that of the parent cyclone from the simulation. Thus, the parent cyclone begins to lose its identity. Now a two-member frontal-cyclone family forms, after the MFC and NFC both advanced to the leading edge of the slow-moving baroclinic zone (see Figs. 8b,c). The cyclone family fits well the description of Bjerknes and Solberg (1922), namely, *each successive member forming to the southwest of its predecessor.* This pattern is also similar to the frontal wave structure shown by Joly and Thorpe (1990).

By 14/12–36, the MFC had deepened from 1000 to 988 hPa in 12 h; it was embedded in a broad southwest–northeast-elongated surface trough (see Fig. 9a). The 36-h simulation appears to be unable to reproduce this elongated trough to the northeast (Fig. 9b). Our detailed analysis of the ship and buoy observations over the region indicates that this elongated trough structure was

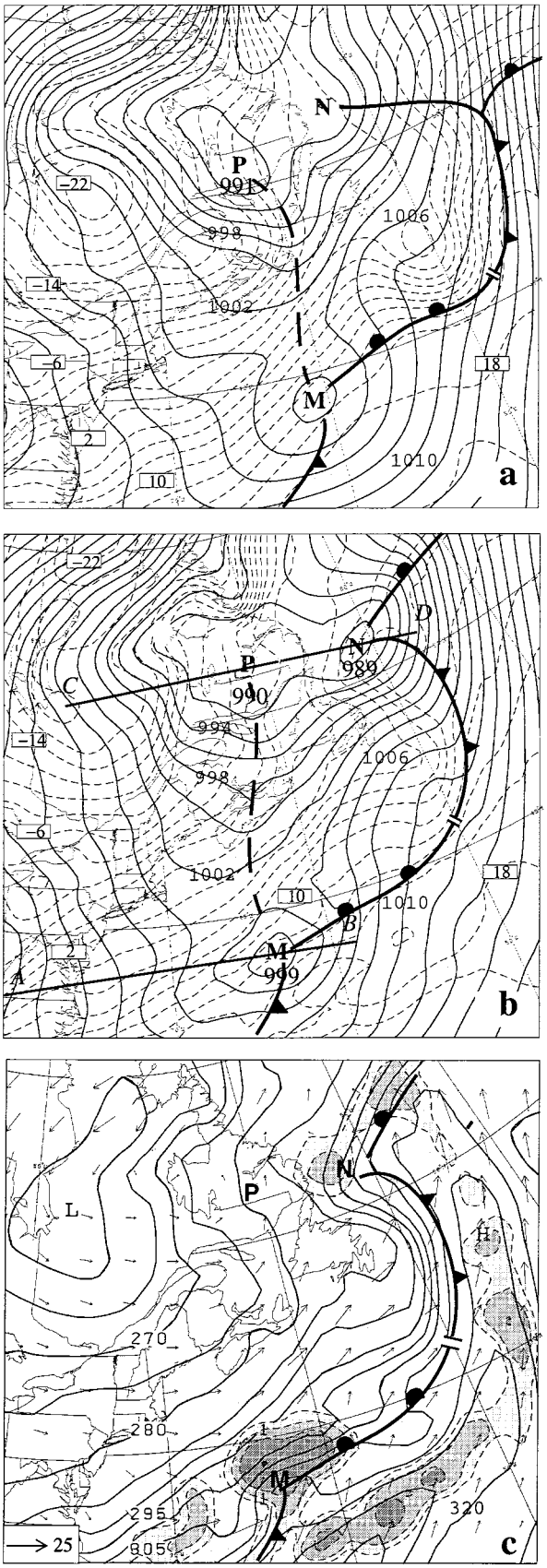

FIG. 8. As in Fig. 6 but for 0000 UTC 14 Mar 1992 (14/00–24).

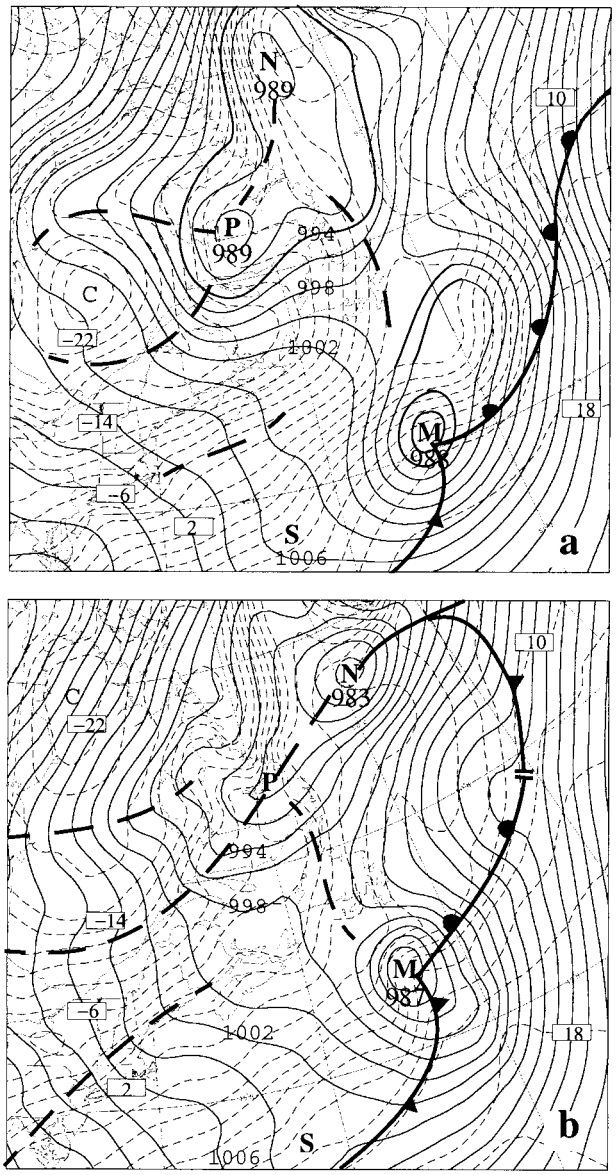

FIG. 9. As in Fig. 6 but for 1200 UTC 14 Mar 1992 (14/12–36). Note that the equivalent potential temperature and wind field are not given.

short lived, about 6–8 h. Nevertheless, the cold–warm frontal structures associated with the MFC in the CMC analysis were well defined. Despite its poorly simulated circulation structure, the model reproduces the observed 12-hPa central pressure drop in 12 h as well as the pertinent cold–warm frontal structures (cf. Figs. 9a,b).

In contrast to the rapid spinup of the MFC, the parent cyclone evolved slowly in both intensity and movement (see Fig. 9). The model appears to produce some slight error in the position and the closed circulation of the parent cyclone, owing likely to the specified northern lateral boundary conditions in which few upper-air observations were available for analysis. Nonetheless, the

model reproduces the intense temperature gradients forced along the ice edge over the northern Labrador Sea (see Figs. 6, 8–10), due to the improved representations of surface conditions over the ice as mentioned in section 2. Furthermore, the model mimics the continued deepening of the NFC (cf. Figs. 9a,b), which meanders over the Labrador Sea due partly to the cyclonic influence of the parent cyclone and partly to the blocking of the low-level flow by the Greenland topography. Of interest at this time is the appearance of a surface short-wave trough, (S), *to the southwest of its predecessor* (i.e., the MFC) in both the analysis and the simulation. *This trough forms again in the cold sector* (cf. Figs. 9 and 10) ahead of a local PV maximum in the PV ring (see Fig. 14b). It tends to amplify in the baroclinic zone and becomes the third member of the frontal-cyclone family, that is, the SFC.

In the following 12 h, the MFC deepened more rapidly than before, that is, at a rate of 14 hPa/12 h (Fig. 5). At 15/00–48, its central pressure dropped to 974 hPa after it moved far to the east of Newfoundland (Fig. 10). It is evident that its associated circulation tended to overwhelm the remnants of the parent low and the NFC, at least in the lower troposphere. Encouragingly, the MFC from the 48-h simulation resembles closely that of the CMC analysis in terms of both intensity and position. In addition, the model replicates very well the cold–warm frontal structures, the thermal ridge wrapping into the cyclone center, and the pressure ridge to the north of the MFC. Similarly, the model captures the weakening and meandering nature of both the parent low and the NFC. Furthermore, it appears to reproduce the intensification of the surface short-wave trough into a closed mesolow, or the SFC (S), its associated cold/warm frontal structures (cf. Figs. 10a,b) and precipitation distribution (cf. Figs. 10c and 12b). Some of the discrepancies between the CMC analysis and the simulation are attributable to the lack of high-resolution surface observations far offshore (see Fig. 1 for the distribution of ship and buoy reports). *The scales of the three-cyclone family range between 500 and 1100 km in diameter (as denoted by the last closed isobar), being spaced at intervals of 1000–1400 km* (between the circulation centers), which are much shorter than those implied by the classical baroclinic theory. These spatial characteristics resemble those described by Reed (1979) and Mullen (1979, 1982). Note the different precipitation structure from the one 24 h earlier (cf. Figs. 8c and 10c). Specifically, the hourly rainfall patterns show the development of more precipitation in the south and to the northwest of the MFC center, but little precipitation farther to the north; they are consistent with the satellite imagery at a later time (see Fig. 12b). Apparently, the precipitating band to the south tends to consume most of the convective available potential energy and available moisture so that the energy supply to the northern region is ''blocked'' (see Figs. 8c and 10c). A model-derived sounding at the cyclone center reveals that all

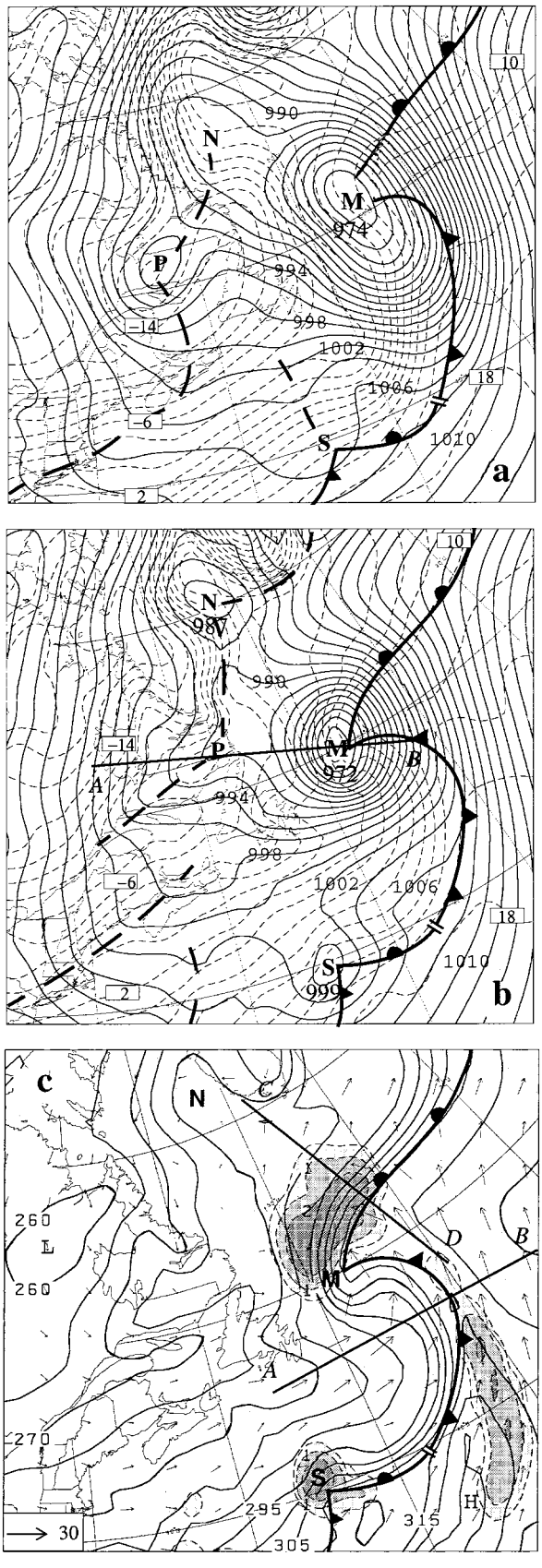

FIG. 10. As in Fig. 6 but for 0000 UTC 15 Mar 1992 (15/00–48).

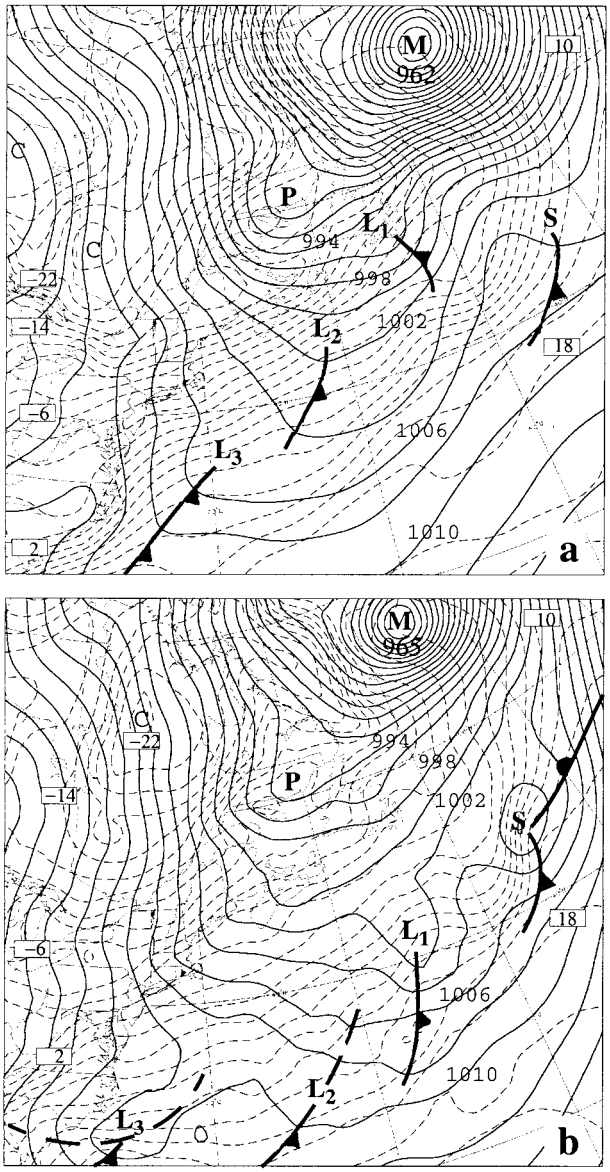

FIG. 11. As in Fig. 6 but for 1200 UTC 15 Mar 1992 (15/12–60). Note that the equivalent potential temperature and wind field are not given. L_1, L_2, and L_3 denote the position of newly formed frontal cyclones.

the rainfall near the MFC center is stratiform in nature with cloud tops located at about 800–600 hPa (Fig. 7b). Note that the sounding structure differs from that at the MFC's incipient stage, which include the presence of weaker vertical shear, more stable and saturated conditions below 800 hPa and less stable above, and a lower tropopause (cf. Figs. 7a,b).

At 15/12–60, both the CMC analysis and the 60-h integration show that the MFC has experienced another 6–7-hPa deepening during the previous 12 h and that it has almost absorbed the circulations associated with the parent cyclone and the NFC to become a robust oceanic cyclone (see Fig. 11). Satellite imagery shows clearly a comma-shaped pattern (Fig. 12b), which is similar to those documented by Reed (1979) and Mullen (1979). The model reproduces reasonably well the basic circulation characteristics of the MFC with respect to its ambient perturbations, indicating the importance of having reliable information from the upstream data-dense region. Subsequently, the system began to fill slowly as it continued its northeastward journey. This weakening is perhaps attributable partly to the ''blocking'' of available high-θ_e air from the south (cf. Figs. 10c and 12b), and partly to its moving away from the parent low pressure zone—a concept to be discussed in the second paragraph that follows. The model also reproduces well the intensity and propagation of the SFC, which has begun to decay with time. Its signal can still be seen from satellite imagery as a small comma cloud mass behind the leading front (cf. Figs. 11 and 12b).

Of special interest is the development of several shortwave perturbations, (L_1), (L_2), and (L_3), *to the southwest behind the leading baroclinic zone* as described by Bjerknes and Solberg (1922); they are superposed again with intense thermal gradients in the vast cold sector (see Figs. 9–11). These baroclinic perturbations can be traced back 12 h earlier (cf. Figs. 10b and 11b) and they seem to correspond roughly to the subsequent three frontal cyclones over the area at 16/12 (see Fig. 13). Their lateral dimensions and circulation structures as well as the processes leading to their genesis appear to be similar to those of the NFC and SFC presented above, since they all develop in the same baroclinically unstable basic state in the cold sector and move along a similar track northeastward from the offshore of North Carolina.

It is worth noting that *the MFC, NFC, and SFC appear to deepen partly at the expense of local available potential energy* (APE) *in the parent cyclone,* seemingly accelerating the weakening of the large-scale system. Specifically, the frontal cyclones tend to *accelerate and experience their central pressure drops,* but not necessarily increase their pressure gradients, as they move from high to low pressure regions (i.e., to the left of the upper-level flow toward the circulation center of the parent cyclone), and then they *decelerate and fill their central pressures* as they move away from the parent cyclone (see Figs. 1, 5, 11, and 13). (The accelerations and decelerations result partly from the conservation of

→

FIG. 12. (a) Infrared satellite imagery at 1801 UTC 14 Mar and (b) visible polar-orbiting satellite imagery at 1533 UTC 15 Mar 1992. The locations of the MFC and SFC are marked by M and S, respectively.

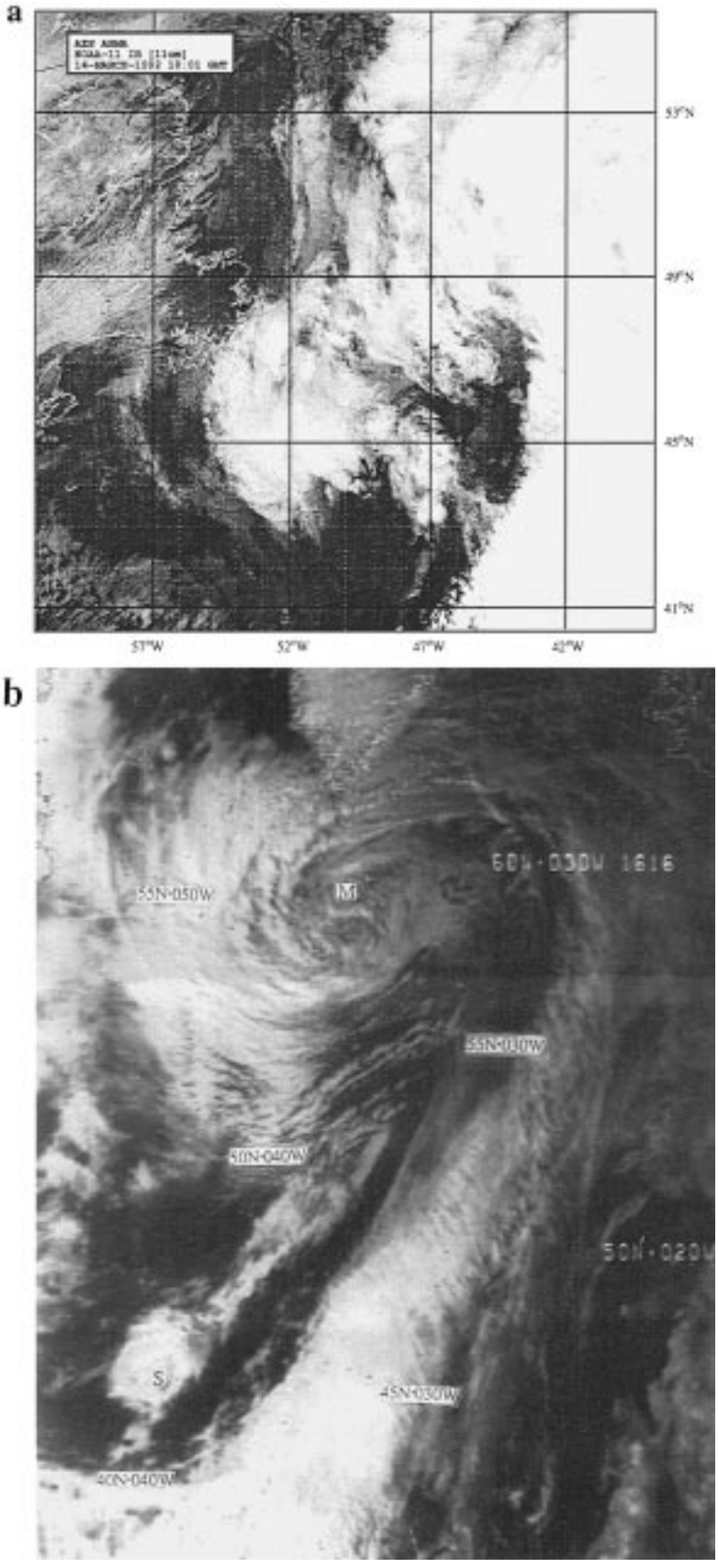
a
53°N
49°N
45°N
41°N
57°W
53°W
49°W
45°W
b
60N-030W 1616
55N-050W
M
55N-030W
50N-040W
50N-020W
S
45N-030W
40N-040W

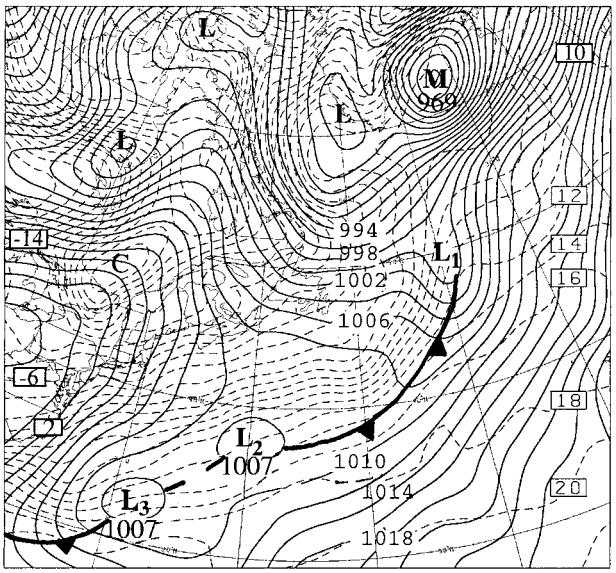

FIG. 13. As in Fig. 2 but for 1200 UTC 16 Mar 1992. L_1, L_2, L_3 denote the newly formed frontal cyclones corresponding to those shown in Fig. 11.

angular momentum of the frontal cyclones with respect to—and partly from their interaction with—the larger-scale sheared steering flow associated with the parent cyclone.) The large central pressure drop, but with a small increase in the circulation intensity, is particularly evident for the NFC, which begins near the isobar of 1005 hPa at a distance of *1400 km to the south* (see Fig. 2b) and ends up with 987 hPa at about *750 km to the northeast* of the parent cyclone center (see Fig. 10). With the 18-hPa central pressure drop the NFC relative vorticity at 900 hPa increases only by 2.3×10^{-5} s^{-1} and its pressure gradient by <1 hPa/100 km. After all, the NFC's central pressure is merely 3 hPa deeper than its outermost closed isobar (Fig. 10b). Similarly, although the MFC deepens 33 hPa in 30 h (at 15/00–48), its central pressure is only 16 hPa deeper than its outermost closed isobar with a pressure gradient of 5 hPa/100 km (Fig. 10b), which is about half the pressure gradient associated with oceanic *bombs* shown in Sanders and Gyakum (1980). Therefore, in addition to the spatial and temporal scales, the intensifying mechanisms and characteristics of the frontal cyclones differ significantly from those typical extratropical cyclones as studied by many previous researchers. Further discussions on the intensifying mechanisms will be given in Part II.

5. Upper-level flow structures

Since there are much less pronounced variations in the upper-level flows than those in the lower levels, we examine only the simulated upper-level flow structures at 15/00–48 in Fig. 14. At this time, the large-scale circulation is still dominated by the parent cyclone to the north. However, it has filled substantially during the previous 48-h period in terms of its depth, the associated pressure gradient, and vorticity concentration (cf. Figs. 3 and 14). Similarly, the westerly jet streak has weakened considerably, that is, from 80 to about 60 m s^{-1}, and its movement slows as it enters a large-scale ridge ahead (see Fig. 14a). The short-wave disturbance T_1, having its trough base located at the left entrance region of the upper-level jet streak, moves slowly eastward. Because of its slow propagation, this trough loses its influence on the MFC genesis as the cyclone moves rapidly northeastward from the entrance to exit regions of the jet streak. Hence, the jet streak–induced indirect circulation, as described by Uccellini and Johnson (1979), may have some positive impact on the deepening of the MFC during its *mature* stage. This impact may be more significant to the *genesis* of the SFC that is now located downstream of the PV ring (cf. Figs. 14a,b).

At this stage, the MFC generates closed circulations at 850 hPa with pronounced cross-isobaric flows and begins to dominate the parent cyclone and the NFC, just as what occurs at the surface (Fig. 14d). Of importance is that the broader area of height deficit induced by the MFC is favorably juxtaposed with the existing thermal structure during the intensifying stage (e.g., Fig. 14d). Specifically, as the MFC moves rapidly into the slowly evolving low-level baroclinic zone, the newly formed height trough is superposed on the intense southwest–northeast-oriented baroclinic zone such that an extensive area of marked cold (warm) advection appears behind (ahead of) the MFC. This scenario occurs because the movement of the MFC appears to be strongly influenced by the PV ring at 400 hPa, whereas that of the thermal trough is most likely determined by the advective process in the lower troposphere. Zhang and Harvey (1995) have shown how a favorable phase relationship between the pressure and thermal waves can be established when a convectively enhanced midlevel trough and a thermal wave propagate at different speeds. In the present case, such a wind–thermal configuration up to 500 hPa is instrumental in the baroclinic conversion of APE into kinetic energy during the MFC genesis, and this is in significant contrast with the benign flows in the vicinity of the other two frontal cyclones (Figs. 14c,d).

To gain additional insight into the baroclinic structures of the frontal cyclones, we examine vertical structures of deviation height and temperature, in association with alongplane wind vectors, through their centers at 14/00–24 (Fig. 15) and 15/00–48 (Fig. 16). During the genesis stage (Fig. 15), the pressure trough associated with the MFC exhibits the typical westward tilt up to 800 hPa; it is under the influence of the upper-level cyclonic flow of the parent cyclone that shows strong vertical shear, again with little vertical tilt (Fig. 15a). Because of its rapid northeastward movement, the MFC is being influenced less by the upper-level short-wave

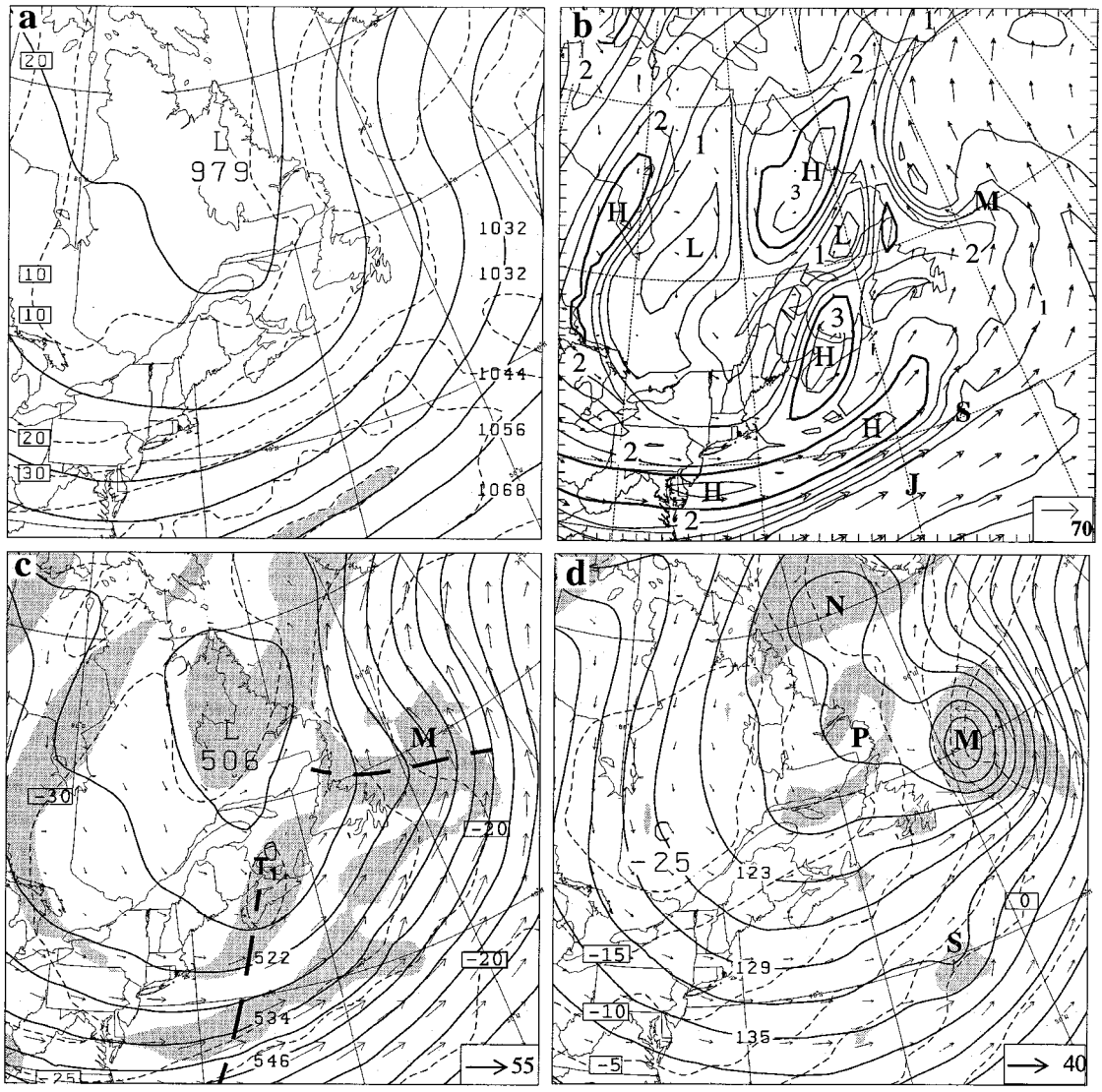

FIG. 14. As in Fig. 3 but from 48-h simulation (15/00–48).

trough (cf. Figs. 3, 4, and 15a). Flow vectors show evidence of warm advection and upward motion along the warm front in the lowest 200 hPa, and a deep layer of moderate cold advection above from the west (cf. Figs. 15a and 8b). On the other hand, the northward advection of high-θ_e air in the warm sector causes the development of near-saturated slantwise ascent and intense precipitation across the warm front, consistent with satellite observations (see Figs. 12a,b). Similar but much weaker and shallower vertical circulations occur in association with the NFC (see Fig. 15b).

By comparison, the parent cyclone is characterized by a vertically coherent trough structure with little horizontal movement, which is consistent with the slow filling of the parent cyclone (see Fig. 15b). The slow movement allows more cold air in the lowest 200 hPa to be advected into the parent cyclone center from the northwest (cf. Figs. 8b and 15b). This tends to elevate the closed circulation of the parent cyclone and lose its identity upward from the surface (Fig. 10). In addition, the movement of the NFC into the Labrador Sea tends to block the source of high-θ_e air from the warm sector (Fig. 8c) and, thus, deprives the parent cyclone of access to the APE through latent heat release.

At 15/00–48, more intense cyclonic circulations, especially in the lowest 300 hPa, occur in the vicinity of the MFC. Of interest is that *the MFC still remains as a low-level shallow system despite the intense latent heat release and the upward extension of cloudiness* to 350 hPa (cf. Figs. 15a and 16). As will be shown in Part II, this shallowness could be attributed to the lack of pronounced upper-level vorticity advection. Strong cross-isobaric convergence into the MFC center, as revealed by flow vectors, leads to the marked concentra-

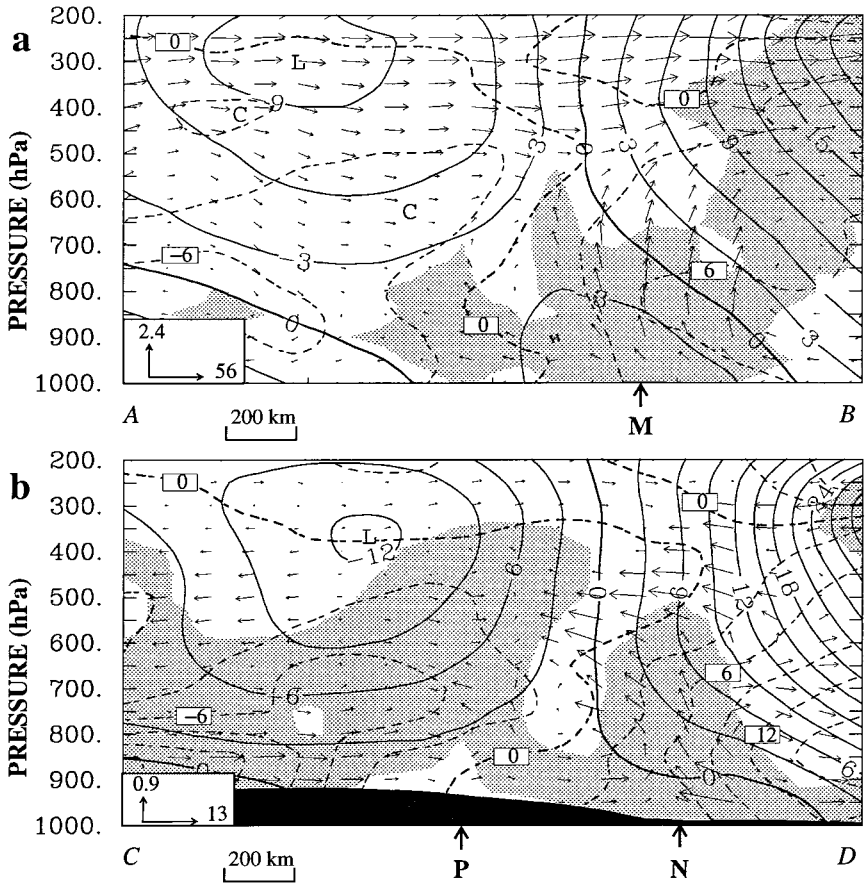

FIG. 15. Vertical cross section of deviation height (solid, every 3 dam) and deviation temperature (dashed, every 3°C), superposed with alongplane wind vectors, which is taken along (a) line AB and (b) line CD given in Fig. 8b from 24-h simulation (14/00–24). The inset indicates the scale of vertical (Pa s^{-1}) and horizontal (m s^{-1}) motions. Shading denotes relative humidity >90%. Locations of the surface low pressure centers are given on the abscissa.

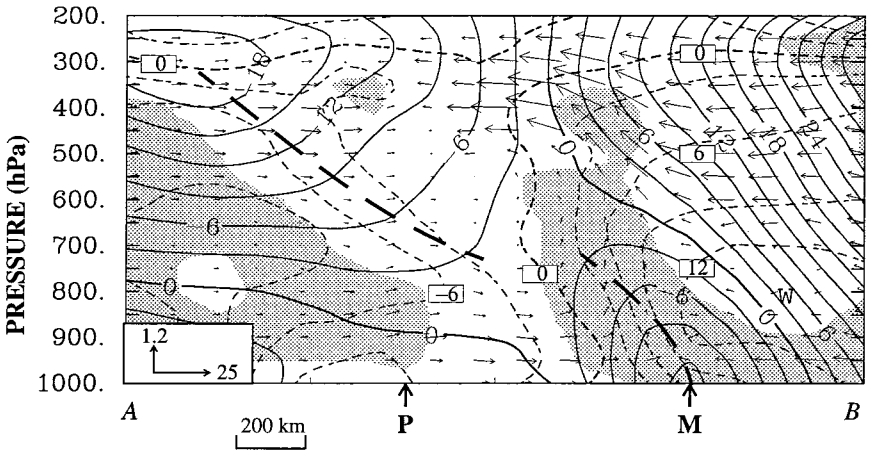

FIG. 16. As in Fig. 15 but from 48-h simulation along line AB given in Fig. 10b.

tion of cyclonic vorticity up to 600 hPa through vortex stretching (cf. Figs. 16 and 17). This convergence also tightens substantially isotherms in a deep layer, with cold (warm) advection behind (ahead of) the MFC (see Figs. 14, 16, and 17), thereby increasing the baroclinic conversion from APE to kinetic energy.

Note that the cyclonic vorticity, convergence zone, and trough axis associated with the MFC all tilt westward, as for a typical large-scale baroclinic wave. Again, the parent cyclone contributes little directly through differential vorticity advection to the deepening of the MFC, since the parent vorticity center at 400 hPa occurs to the far west of the MFC (Fig. 17). Rather, a deep layer (i.e., from 600 to 250 hPa) of cyclonic vorticity ($>10 \times 10^{-5}$ s^{-1}) is advected into the MFC region from behind by cyclonic (southeasterly in the cross section) flows (20–30 m s^{-1}). This positive vorticity layer corresponds to the ring of high PV on the cyclonic side of the upper-level jet streak (cf. Figs. 14b and 17). Note also that the near-saturated slantwise ascent that occurs up to 350 hPa in the vicinity of the MFC, as shaded in Figs. 10c and 16. This slantwise ascent draws high-θ_e air from the boundary layer in the warm sector where little or no upward motion is present, and then lifting to saturation takes place in the convergent flow. It is evident that latent heat release must play an important role in the rapid deepening of the MFC (and the other two frontal cyclones), since more intense precipitation occurs in close proximity to their centers (Hack and Schubert 1986).

Finally, Figs. 18a,b show vertical structures of equivalent potential temperature (θ_e) and cross-frontal flows across the cold and warm fronts of the MFC in order to facilitate the understanding of the roles of moist dynamics in the frontal cyclogenesis. The cold front is characterized by a deep layer of descent to its rear, a sharp change to ascent along the nearly upright frontal zone, an intense updraft in a narrow zone ahead, and a weak vertical motion in the warm sector. The θ_e structure exhibits the presence of potential instability ahead of the cold front, and it is released partly near the frontal zone in the form of deep convection. As mentioned previously, the potential instability is established as a result of the transport of tropical high-θ_e maritime boundary layer air by the low-level intensifying flow that is enhanced by upward sensible and latent heat fluxes from the warm ocean (see Fig. 10c). Note the quite different low-level θ_e profiles across the cold front, namely, a deep well-mixed θ_e layer (up to 800 hPa) behind the front that is generated by strong upward surface fluxes of sensible and latent heat in the cold air mass overlying the warm ocean water, and a shallow layer of the stratified warm air mass ahead with little horizontal thermal gradient and little vertical coupling except in the intense updraft zone.

In contrast, *slantwise* convection appears to be the mechanism by which latent heat is released along the warm front. This can be seen from the distribution of three-dimensional moist potential vorticity, given in Fig. 18b, which shows near-vanishing to negative values in the near-saturated sloping flow. This implies the presence of moist symmetric instability along the warm front, as has also been noted by Kuo and Reed (1988), Reuter and Yau (1990), and Huo et al. (1995) in association with large-scale warm front. The little upward motion in the warm sector but pronounced sloping ascent over the frontal zone suggests that the moist symmetric unstable air is being transported by the southerly flow into the frontal region, where lifting to saturation occurs and the instability is released. This is consistent with the simulated precipitation structures (see Figs. 8c and 10c).

6. Summary and concluding remarks

In this study, an improved version of MM4, the PSU–NCAR hydrostatic, nested-grid, mesoscale model is utilized to study a family of frontal cyclones that occurred over the western Atlantic Ocean during 13–15 March 1992, with a fine-mesh grid size of 30 km. A total of six frontal cyclones deepened successively near the leading edge of a large-scale frontal zone with their decaying parent cyclone located in the polar region. They have a diameter of 500–1100 km (as denoted by the last closed isobar) and are spaced 1000–1400 km apart (between the circulation centers). One of the frontal cyclones (i.e., MFC) underwent explosive deepening, that is, at a rate of 44 hPa/42 h, and it eventually overpowered the parent cyclone. Most operational numerical weather prediction models still have great difficulty predicting the development of such mesocyclones, as in the present case.

Although the model is initialized with conventional observations, it demonstrates reasonable capability up to 60 h in reproducing the genesis, track, and intensity of the frontal cyclones including the MFC, NFC, and SFC, their associated thermal structure and precipitation pattern, as well as their surface circulations, as verified against the CMC analysis and other available observations. Table 1 summarizes the basic characteristics of the frontal-cyclone family. The model also captures well the quasi-stationary and slow decaying nature of the parent cyclone, which is characterized by a deep coherent baroclinic structure in the vertical.

It is shown that *all the frontal cyclones form successively to the southwest of their predecessors in the cold air mass on the cyclonic side of the jet streak behind the slow-moving large-scale cold front.* They first appear as pressure troughs superposed on a baroclinically unstable basic state (i.e., with strong vertical wind shear) but have little tendency to amplify. Then, *the genesis occurs as a result of baroclinic energy conversion in a shallow layer of weak static stability in the lower troposphere, as moving over the warm Gulf Stream water toward the leading large-scale frontal zone.* Subsequently, the frontal cyclones deepen rapidly through la-

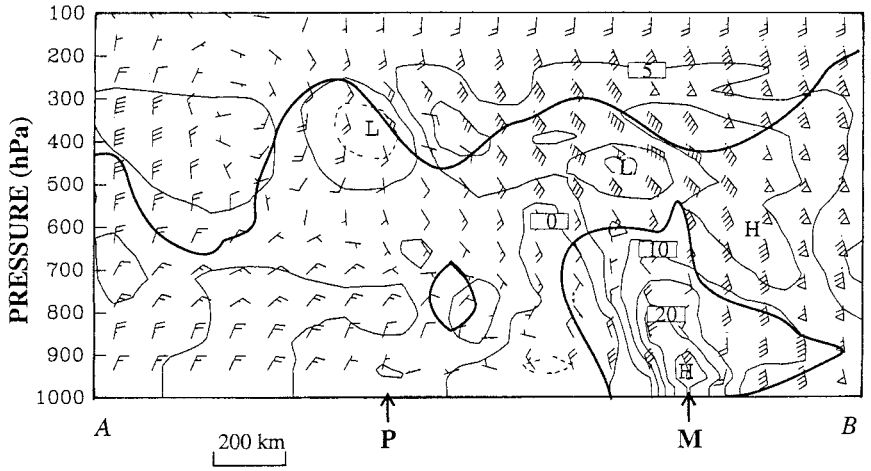

FIG. 17. As in Fig. 16 but for relative vorticity (solid is positive, dashed is negative) at intervals of 5×10^{-5} s^{-1}, superposed with wind barbs. A full (half) barb is 5 (2.5) m s^{-1} and a pennant is 25 m s^{-1}. Thick solid line represents PV of 2 PVU.

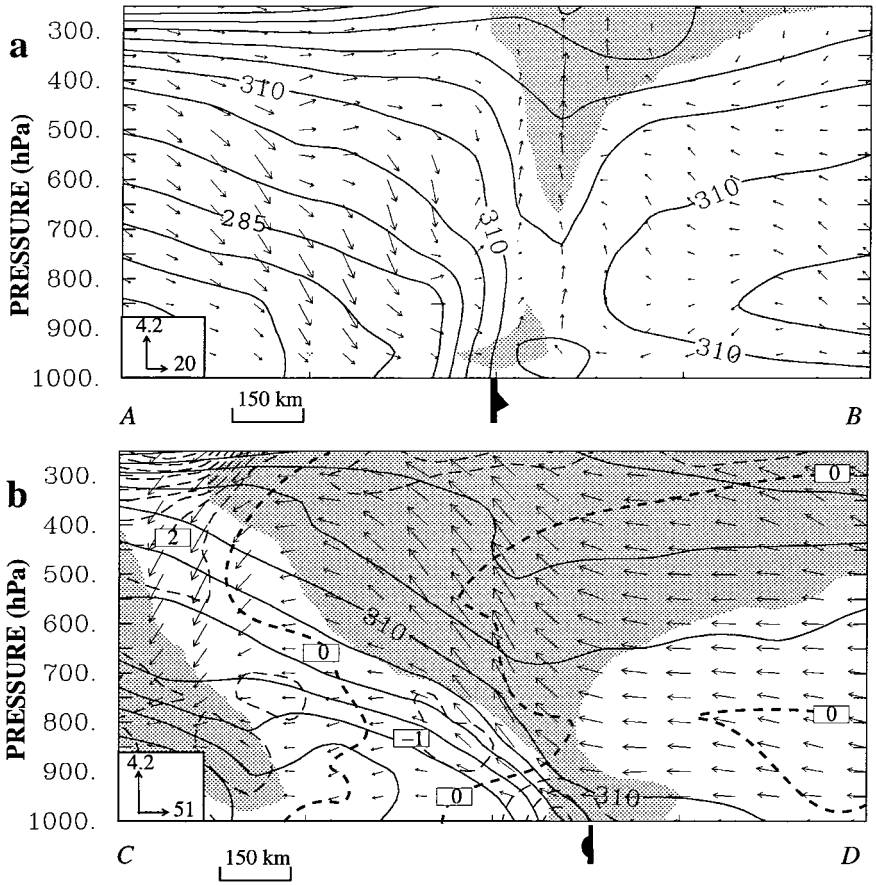

FIG. 18. As in Fig. 16 but for equivalent potential temperature (solid) at intervals of 5 K and moist potential vorticity (dashed), superposed with alongplane flow vectors, which is taken along (a) line AB and (b) line CD given in Fig. 10c. Thick dashed line denotes areas with negative moist potential vorticity.

TABLE 1. The initiation times, maximum deepenings, and lifetimes of individual frontal cyclones inferred from the CMC analysis and the 60-h simulation.

Frontal cyclone identifier	Initiation time (date/hour)	Initiation location (lat–long)	Lifetime (days)	Total deepening (hPa)
M	prior to 10/12	59°N, 110°W	>7	44
N	prior to 10/12	35°N, 73°W	>2.5	20
S	14/12	36°N, 62°W	>1	4
L_1	15/00	40°N, 63°W	>1.5	5
L_2	15/12	34°N, 70°W	>1	3
L_3	15/12	33°N, 75°W	>1	2

tent heat release in their own circulations after passing over the warm water. It is found that the MFC could be traced back 2.5 days earlier, like a ''polar low'' in the cold air mass over northern Alberta. Once it moves offshore, the MFC accelerates from 15 to 25 m s^{-1} towards the parent cyclone center by the large-scale cyclonic steering flow. Little precipitation is generated during the genesis stage, suggesting that the dry dynamics determines the genesis of each frontal cyclone. Once they intensify, these secondary cyclones begin to establish their own mesoscale cold–warm frontal circulations, thus distorting the leading large-scale frontal structures. This distortion alters gradually the distribution and type of precipitation, namely, mostly convective (stratiform) along the newly formed cold (warm) fronts, rather than mostly convective along the original cold front. More pronounced precipitation occurs in the vicinity of the MFC, in agreement with its more rapid amplification. It is also found that *these secondary cyclones are indeed shallow in their vertical extent, with a pressure thickness ranging from 150 hPa (for the NFC) to 300 hPa (for the MFC).* The average *e*-folding time for the MFC is about 22 h. At the end of the 60-h integration, the model simulates several short-wave disturbances in the cold sector behind the primary cold front, which correspond well to the subsequent development of three new frontal cyclones seen in the CMC analysis.

It is found that *all the frontal cyclones, including the MFC, NFC, and SFC, deepen partly at the expense of local APE in the parent cyclone, thus speeding up the dissipation of the large-scale system.* They tend to gain angular momentum and experience their central pressure drops as they move from high to low pressure regions toward the center of the parent cyclone, and they decelerate and fill as they move away from the parent cyclone. Furthermore, *a ring of upper-level PV anomalies on the cyclonic side of the jet streak appears to assist the genesis and steer the movement of the frontal cyclones.* Thus, the decaying parent cyclone provides a favorable large-scale environment for secondary cyclogenesis, at least through reduced pressures toward its center. It follows that frontal cyclones are indeed different in character (e.g., vertical extent, spatial and temporal scales) and in intensifying mechanisms from those typical extratropical cyclones as studied by previous researchers.

Acknowledgments. We are grateful to Lance Bosart for his continuous interest and support. The computations were performed at the National Center for Atmospheric Research, which is sponsored by the National Science Foundation (NSF). This work was supported by Atmospheric Environment Service of Canada, NSF ATM-9413012, and ATM-9802391.

REFERENCES

Anthes, R. A., E.-Y. Hsie, and Y.-H. Kuo, 1987: Description of the Penn State/NCAR mesoscale model version 4 (MM4). NCAR Tech. Note NCAR/TN-282, 66 pp.

Benjamin, S. G., and N. L. Seaman, 1985: A simple scheme for objective analyses in curved flow. *Mon. Wea. Rev.,* **113,** 1184–1198.

Bjerknes, J., and H. Solberg, 1922: Life cycle of cyclones and the polar front theory of atmospheric circulation. *Geofys. Publ.,* **3** (1), 1–18.

Bosart, L. F., and F. Sanders, 1991: An early-season coastal storm: Conceptual success and model failure. *Mon. Wea. Rev.,* **119,** 2831–2851.

Browning, K. A., and N. M. Roberts, 1994: Structure of a frontal cyclone. *Quart. J. Roy. Meteor. Soc.,* **120,** 1535–1557.

——, and B. W. Golding, 1995: Mesoscale aspects of a dry intrusion within a vigorous cyclone. *Quart. J. Roy. Meteor. Soc.,* **121,** 463–493.

Charney, J. G., 1947: The dynamics of long waves in a baroclinic westerly current. *J. Meteor.,* **4,** 135–162.

Dudhia, J., 1989: Numerical study of convection observed during the winter monsoon experiment using a mesoscale two-dimensional model. *J. Atmos. Sci.,* **46,** 3077–3107.

Eady, E. T., 1949: Long waves and cyclone waves. *Tellus,* **1,** 33–52.

Ford, R. P., and G. W. K. Moore, 1990: Secondary cyclogenesis—Comparison of observations and theory. *Mon. Wea. Rev.,* **118,** 427–446.

Hack, J. J., and W. H. Schubert, 1986: Nonlinear response of atmospheric vortices to heating by organized cumulus convection. *J. Atmos. Sci.,* **43,** 1559–1573.

Harrold, T. W., and K. A. Browning, 1969: The polar low as a baroclinic disturbance. *Quart. J. Roy. Meteor. Soc.,* **95,** 710–723.

Hoskins, B. J., 1990: Theory of extratropical cyclones. *Extratropical Cyclones: The Erik Palmén Memorial Volume,* C. W. Newton and E. O. Holopainen, Eds., Amer. Meteor. Soc., 64–80.

——, M. E. Mcintyre, and R. W. Robertson, 1985: On the use and significance of isentropic potential vorticity amps. *Quart. J. Roy. Meteor. Soc,* **111,** 877–946.

Hsie, E.-Y., R. A. Anthes, and D. Keyser, 1984: Numerical simulation of frontogenesis in a moist atmosphere. *J. Atmos. Sci.,* **41,** 2581–2594.

Huo, Z., D.-L. Zhang, J. R. Gyakum, and A. Staniforth, 1995: A diagnostic analysis of the superstorm of March 1993. *Mon. Wea. Rev.,* **123,** 1740–1761.

Joly, A., and A. J. Thorpe, 1990a: The stability of a steady horizontal

shear front with uniform potential vorticity. *J. Atmos. Sci.,* **47,** 2612–2622.

——, and ——, 1990b: Frontal instability generated by tropospheric potential vorticity anomalies. *Quart. J. Roy. Meteor. Soc.,* **116,** 525–560.

——, and Coauthors, 1997: The Fronts and Atlantic Storm-Track Experiment (FASTEX): Scientific objectives and experimental design. *Bull. Amer. Meteor. Soc.,* **78,** 1917–1940.

Kain, J. S., and J. M. Fritsch, 1990: A one-dimensional entraining/detraining plume model and its application in convective parameterization. *J. Atmos. Sci.,* **47,** 2784–2802.

——, and ——, 1993: Convective parameterization for mesoscale models: The Kain–Fritsch scheme. *The Representation of Cumulus Convection in Numerical Models, Meteor. Monogr.,* No. 46, Amer. Meteor. Soc., 165–170.

Kasahara, A., and D. B. Rao, 1972: Instabilities of frontal motions in the atmosphere. *J. Atmos. Sci.,* **29,** 1090–1108.

Kuo, Y.-H., and R. J. Reed, 1988: Numerical simulation of an explosively deepening cyclone in the eastern Pacific. *Mon. Wea. Rev.,* **116,** 2081–2105.

Matsumoto, S., S. Yoshizumi, and M. Takeuchi, 1970: On the structure of the ''Baiu-Front'' and the associated intermediate scale disturbances in the low atmosphere. *J. Meteor. Soc. Japan,* **48,** 479–491.

Moore, G. K. W., and W. R. Peltier, 1987: Cyclogenesis in frontal zones. *J. Atmos. Sci.,* **44,** 384–409.

——, and ——, 1990: Nonseparable baroclinic instability. Part II: Primitive-equations dynamics. *J. Atmos. Sci.,* **47,** 1223–1242.

Mullen, S. L., 1979: An investigation of small synoptic-scale cyclones in polar air streams. *Mon. Wea. Rev.,* **107,** 1636–1647.

——, 1982: Cyclone development in polar air streams over the wintertime continent. *Mon. Wea. Rev.,* **110,** 1664–1676.

Nakamura, N., 1988: Scale selection of baroclinic instability—Effects of stratification and nongeostrophy. *J. Atmos. Sci.,* **45,** 3253–3267.

O'Handley, C., and L. F. Bosart, 1996: The impact of the Appalachian Mountains on cyclonic weather system. *Mon. Wea. Rev.,* **124,** 1353–1373.

Orlanski, I., 1968: Instability of frontal waves. *J. Atmos. Sci.,* **25,** 178–200.

——, 1975: A rational subdivision of scales for atmospheric processes. *Bull. Amer. Meteor. Soc.,* **56,** 527–530.

——, 1986: Localized baroclinicity: A source for meso-α cyclones. *J. Atmos. Sci.,* **43,** 2857–2885.

Parker, D. J., 1998: Secondary frontal waves in the North Atlantic region: A dynamical perspective of current ideas. *Quart. J. Roy. Meteor. Soc.,* **124,** 829–856.

Perkey, D. J., and C. W. Keitzberg, 1976: A time-dependent lateral boundary scheme for limited-area primitive equation models. *Mon. Wea. Rev.,* **104,** 744–755.

Rasmussen, E., 1981: An investigation of a polar low with a spiral cloud structure. *J. Atmos. Sci.,* **38,** 1785–1792.

Reed, R. J., 1979: Cyclogenesis in polar air streams. *Mon. Wea. Rev.,* **107,** 38–52.

——, 1990: Advances in knowledge and understanding of extratropical cyclones during the past quarter century: An overview. *Extratropical Cyclones: The Erik Palmén Memorial Volume,* C. W. Newton and E. O. Holopainen, Eds., Amer. Meteor. Soc., 27–45.

Reuter, G. W., and M. K. Yau, 1990: Observations of slantwise convective instability in winter cyclones. *Mon Wea. Rev.,* **118,** 447–458.

Sanders, F., and J. R. Gyakum, 1980: Synoptic-dynamic climatology of the ''bomb.'' *Mon. Wea. Rev.,* **108,** 1589–1606.

Schär, C., and H. Davies, 1990: An instability of mature cold fronts. *J. Atmos. Sci.,* **47,** 929–950.

Snyder, C., 1996: Summary of an informal workshop on adaptive observations and FASTEX. *Bull. Amer. Meteor. Soc.,* **77,** 953–961.

Stewart, R. E., 1991: Canadian Atlantic Storm Program: Progress and plans of the meteorological component. *Bull. Amer. Meteor. Soc.,* **72,** 364–371.

Thorncroft, C. D., and B. J. Hoskins, 1990: Frontal cyclogenesis. *J. Atmos. Sci.,* **47,** 2317–2336.

Uccellini, L. W., 1990: Processes contributing to the rapid development of extratropical cyclones. *Extratropical Cyclones: The Erik Palmén Memorial Volume,* C. W. Newton and E. O. Holopainen, Eds., Amer. Meteor. Soc., 81–105.

——, and D. R. Johnson, 1979: The coupling of upper- and lower-tropospheric jet streaks and implications for the development of severe convective storms. *Mon. Wea. Rev.,* **107,** 682–703.

——, and P. J. Kocin, 1987: The interaction of jet streak circulations during heavy snow events along the east coast of the United States. *Wea. Forecasting,* **2,** 298–308.

Wang, P.-Y., J. E. Martin, J. D. Locatelli, and P. V. Hobbs, 1995: Structure and evolution of winter cyclones in the central United States and their effects on the distribution of precipitation. Part II: Arctic fronts. *Mon. Wea. Rev.,* **123,** 1328–1344.

Yoshizumi, S., 1977: On the structure of intermediate-scale disturbances on the Baiu front. *J. Meteor. Soc. Japan,* **55,** 107–120.

Zhang, D.-L., 1989: The effect of parameterized ice microphysics on the simulation of vortex circulation with a mesoscale hydrostatic model. *Tellus,* **41A,** 132–147.

——, and R. A. Anthes, 1982: A high-resolution model of the planetary boundary layer—Sensitivity tests and comparisons with SESAME-79 data. *J. Appl. Meteor.,* **21,** 1594–1609.

——, and R. Harvey, 1995: Enhancement of extratropical cyclogenesis by a mesoscale convective system. *J. Atmos. Sci.,* **52,** 1107–1127.

——, H.-R. Chang, N. L. Seaman, T. T. Warner, and J. M. Fritsch, 1986: A two-way interactive nesting procedure with variable terrain resolution. *Mon. Wea. Rev.,* **114,** 1330–1339.

——, E. Radeva, and J. Gyakum, 1999: A family of frontal cyclones over the western Atlantic Ocean. Part II: Parameter studies. *Mon. Wea. Rev.,* **127,** 1745–1760.